The Effect of Argon Ion Beam Irradiation Post-Deposition Treatment on the Thickness and Structure of Ultrathin Amorphous Carbon Films for Magnetic Storage Technology

J. Xie and K. Komvopoulos
Department of Mechanical Engineering, University of California, Berkeley, CA 94720, USA

Abstract

Carbon films synthesized by plasma-enhanced chemical vapor deposition (PECVD) and filtered cathodic vacuum arc (FCVA) exhibit multi-layer structures consisting of interface and surface layers rich in sp^2 atomic carbon bonding and intermediate (bulk) layer of much higher sp^3 content. Because of significant differences in the composition, structure, and thickness of these layers, decreasing the film thickness may negatively impact the film quality. In this study, Ar^+ ion beam irradiation post-deposition treatment was used to reduce the thickness and enhance the structure uniformity of carbon films. Transmission electron microscopy (TEM) and electron energy loss spectroscopy (EELS) were used to examine the effect of Ar^+ ion beam irradiation on the structure and thickness of ultrathin films of hydrogenated amorphous carbon (*a*-C:H) and hydrogen-free amorphous carbon (*a*-C) deposited by PECVD and FCVA, respectively. The TEM and EELS results indicate that 2-min ion beam irradiation decreases the film thickness without markedly changing the film structure and composition; however, 4-min ion beam irradiation produces significant film thinning and moderately decreases the sp^3 content of the bulk layer. The results of this study demonstrate that Ar^+ ion beam irradiation is an effective post-deposition process for reducing the thickness and tuning the structure of PECVD and FCVA *a*-C films. This capability has direct implications in the synthesis of ultrathin protective overcoats for extremely-high-density magnetic recording.

I. INTRODUCTION

Amorphous carbon (*a*-C) films are used as protective overcoats in numerous industrial applications, mainly because they exhibit unique mechanical properties and good chemical stability. The characteristics of *a*-C films strongly depend on the dominance of trigonal (sp^2) or tetrahedral (sp^3) atomic carbon hybridization. In general, dense and hard *a*-C films possess high sp^3 contents. The type of atomic carbon hybridization in *a*-C films greatly depends on the process conditions and method of film deposition. Plasma-enhanced chemical vapor deposition (PECVD) and filtered cathodic vacuum arc (FCVA) are effective methods for depositing ultrathin *a*-C films [1–3]. However, the structure, thickness, and properties of the *a*-C films deposited by these methods may significantly vary due to fundamental differences in film growth conditions.

Ultrathin *a*-C films are of particular importance in storage technology, where they are extensively used as protective overcoats of magnetic media and heads. In response to constantly increasing demands for even higher storage densities in magnetic recording, the distance between the magnetic medium of the hard disk and the read/write transducer embedded at the trailing edge of the head has been greatly reduced in contemporary hard-disk drives. This has been largely accomplished by depositing ultrathin *a*-C overcoats on the disk and head media mainly by PECVD and FCVA techniques [1–5]. However, extremely small thickness may negatively impact the protective capability of the overcoat. Considering the existence of chemical and structural gradients through the thickness of *a*-C films, which result in a multi-layer cross-sectional structure consisting of interface, bulk, and surface layers with markedly different structures and thicknesses [6–8], excessive overcoat thinning may yield media with significantly altered mechanical, tribological, and corrosion characteristics. In particular, the decrease of the overcoat thickness may come at the expense of the sp^3-rich bulk layer. An ultrathin (<5 nm) *a*-C film with a very thin bulk layer of thickness comparable to those of the sp^2-rich interface and surface layers implies a decrease in film density and mechanical strength and, presumably, inadequate corrosion and wear

resistance. Therefore, reducing the *a*-C film thickness without degrading its protective capability is of paramount importance in contemporary magnetic recording technology.

Ion beam irradiation is a promising post-deposition method for decreasing the overcoat thickness and tuning the film structure *in situ*. Previous studies dealing with post-growth film treatment have focused on the effect of surface modification on the overall film properties. For example, Cheah et al. [9] reported that ion beam irradiation of tetrahedral *a*-C films increased the sp^3 content and the density of sp^3-rich nanoclusters having sp^2-rich boundaries. Patsalas and Logothetidis [10,11] irradiated sputtered *a*-C films with 0.5- and 1.5-keV Ar^+ ion beams and observed that sp^2-rich *a*-C films deposited under floating substrate bias exhibited surface smoothing, densification, and diamond crystallization, whereas sp^3-rich *a*-C films deposited under negative substrate bias voltage demonstrated relatively less change. Silinskas and Grigonis [12] reported that exposure of hydrogenated *a*-C (*a*-C:H) films to low energy (0.1–0.7 keV) Ar^+ ion beams caused damage to the graphite clusters and sputter etching of the graphite phase; in particular, *a*-C:H films of thickness <300 nm became more diamond-like and their graphite clusters exhibited more disordering. Vinnichenko et al. [13] observed that 15-min Ar^+ ion beam irradiation of 10-nm-thick *a*-C films deposited by FCVA under a substrate bias voltage of –500 V decreased the film thickness without altering the surface roughness.

The aforementioned studies and several others in the literature indicate that understanding of the effect of Ar^+ ion beam irradiation on the structure and thickness of ultrathin *a*-C films is rather sparse. In particular, a comprehensive study of the changes in carbon atom hybridization and thickness of interface, bulk, and surface structural layers of *a*-C films of thickness <5 nm due to the effect of ion beam irradiation has not been performed yet. Such study requires the use of high-resolution techniques, such as transmission electron microscopy (TEM) and electron energy loss spectroscopy (EELS). The high spatial and energy resolution of EELS makes it suitable for measuring the atomic carbon distribution and sp^3 content through the thickness of ultrathin *a*-C films and, consequently, identify changes in the structure and thickness of structural layers.

The objective of this investigation is to elucidate the effect of Ar^+ ion beam irradiation on the thickness and structure of ultrathin carbon films deposited by PECVD and FCVA. Changes in through-thickness carbon concentration and hybridization as well as film thickness were studied by high-resolution TEM (HRTEM) and cross-sectional EELS. Results from these analyses are contrasted to show differences between ultrathin films deposited by PECVD and FCVA, elucidate the effect of Ar^+ ion beam irradiation on the quality of the produced films, and provide insight into the decrease of film thickness by post-deposition Ar^+ ion beam irradiation.

II. EXPERIMENTAL PROCEDURES

A. Film synthesis

Glass disks of 2.5-in. diameter coated with a ~100-nm-thick NiTa layer were cut into 1×1 cm^2 pieces, which were then used as substrates. Ultrathin (~5 nm) *a*-C:H films were deposited onto the NiTa/glass substrates by PECVD using acetylene (C_2H_2) as the film precursor. The density (obtained from X-ray reflectivity measurements using a standard procedure) and hydrogen content of the PECVD *a*-C films, as determined by the manufacturer, are equal to ~2.0–2.1 g/cm^3 and 30–40 at%, respectively. To deposit *a*-C films on similar substrates by FCVA, NiTa/glass substrates coated with a PECVD *a*-C film were loaded onto the substrate stage of a custom-made FCVA system [14,15] and the film was removed by sputter etching with a 500-eV Ar^+ ion beam generated by a 64-mm Kaufman ion source (Commonwealth Scientific, Alexandria, VA) at a working pressure of ~2×10^{-4} Torr and Ar^+ ion incidence angle (measured from the normal to the substrate surface) equal to 60°. Under these sputtering conditions, the PECVD *a*-C film is completely removed after 6 min of Ar^+ ion bombardment [16]. After allowing the chamber to cool down for 5 min and the base pressure to decrease to $<5 \times 10^{-7}$ Torr, plasma arcing at the cathode (99.99% pure graphite) surface was initiated by a mechanical striker, while the substrate stage was oriented normal to the C^+ ion flux. An optimum pulsed bias voltage of –100 V and frequency of 25 kHz was used to control the C^+ ion energy during film synthesis by FCVA. To produce

ultrathin *a*-C films of similar thickness with those deposited by PECVD, the deposition time was fixed at 12 s. For uniform sputter etching and film deposition in the radical direction, the substrate stage was rotated at 60 rpm during both ion beam irradiation and FCVA deposition. More details about the FCVA system and deposition process can be found elsewhere [14–17].

B. Post-deposition ion beam irradiation

The *a*-C films were sputter etched in the same FCVA chamber with a 500-eV Ar^+ ion beam under a working pressure of ~2×10^{-4} Torr and ion beam incidence angle (measured from the normal to the substrate surface) equal to 60°. The beam voltage was fixed at 17 mA, while the etching time was set equal to 2 or 4 min.

C. Analytical methods

Cross-sectional HRTEM samples were prepared by mechanical grinding, dimpling, and surface finishing by ion milling. To distinguish the epoxy glue from the *a*-C film and to separate the EELS carbon signals originating from the carbon film and the carbon-based epoxy glue, a thin (5–10 nm) Au capping layer was sputtered onto the surface before sample bonding. Further details about the TEM sample preparation method used in this study can be found elsewhere [16,18,19].

HRTEM images and EELS spectra were obtained with a FEI Tecnai (F20 UT) microscope operated at 200 kV, using a CCD camera (2048 × 2048 pixels) positioned 42 mm behind the Gatan imaging filter. A 150-µm C2 aperture, a 9.4-mrad C2 semi-angle, and an EELS collection semi-angle of 16.3 mrad were used in all the measurements. The spatial resolution of the scanning TEM (without a monochromator) is 0.14 nm. Because the band gap difference between sp^2 and sp^3 is about 0.8–0.9 eV, the available energy resolution of ≤0.58 eV (determined from the full-width at half-maximum of the zero-loss peak) is sufficiently low for distinguishing the sp^2 from sp^3 hybridizations.

III. RESULTS AND DISCUSSION

To determine the amount of carbon removed by Ar^+ ion sputter etching, cross-sectional TEM samples obtained before and after Ar^+ ion beam irradiation for 2 and 4 min were examined. Fig. 1 shows cross-sectional HRTEM images of as-deposited and Ar^+ ion irradiated specimens coated with *a*-C films deposited by PECVD. The *a*-C/NiTa and *a*-C/Au interfaces are indicated by dashed lines. The different material layers through the specimen thickness are labeled in Fig. 1(b). The images reveal a layered cross-sectional structure consisting of (1) NiTa layer, (2) *a*-C film, (3) Au capping layer, and (4) epoxy glue [Fig. 1(b)]. The average film thickness measured from the TEM images shown in Fig. 1 is given in Table 1. Sputter etching during Ar^+ ion beam irradiation for 2 and 4 min reduced the average film thickness of PECVD *a*-C films was from 4.6 to 2.8 and 1.1 nm, respectively. Thus, for the present Ar^+ ion irradiation conditions, the average etching rate of the PECVD *a*-C films estimated from HRTEM images is equal to ~0.9 nm/s.

A detailed examination of the cross-sectional elemental composition of the PECVD *a*-C films was performed by EELS. With this technique, the chemical composition and structure of materials can be determined by measuring the energy loss of electrons passing through the specimen due to inelastic electron-electron collisions [20,21]. Beam electrons interacting with inner (core-shell) electrons of the specimen material are detected in the high-energy-loss range (>50 eV) of the EELS spectrum. The sp^2 and sp^3 film contents can be determined from the characteristic K-edge spectrum in the range of 280–305 eV. Specifically, the pre-edge peak at 285 eV is due to electron excitation from the ground-state 1s core level to the vacant π^*-like anti-bonding states, whereas the peak starting at 290 eV is due to electron excitation from the 1s core level to the σ^*states. Therefore, information about the elemental composition can be extracted from the ionization edges. The π^* peak is fitted with a Gaussian distribution, while the σ^* peak is integrated over the energy window from 290 to 305 eV to minimize plural scattering effects.

Assuming that the area ratio of the two peaks is proportional to the relative number of π^* and σ^* orbitals, i.e., 0/4 for 100% sp^3 and 1/3 for 100% sp^2, the fraction of sp^2 bonded carbon atoms x in the film is given by [22]

$$\frac{(\pi^*/\sigma^*)_{\text{film}}}{(\pi^*/\sigma^*)_{\text{std}}} = \frac{3x}{4-x} \tag{1}$$

where the standard (std) sample consists of 100% sp^2 evaporated carbon. More details about the curve fitting method and calculation of sp^3 fraction can be found elsewhere [8].

A comparison of the EELS results shown in Fig. 2 shows the effect Ar^+ ion beam irradiation on the structure of *a*-C films deposited by PECVD. Because 4-min Ar^+ ion irradiation yielded low carbon intensity, only results for 2-min Ar^+ ion irradiation are included in Fig. 2(b). The normalized carbon intensity was obtained by integrating the EELS spectrum from 280 to 305 eV and then dividing it by the maximum carbon intensity, whereas the sp^3 depth profiles were determined from the C K-edge spectra using Eq. (1). The vertical dashed lines indicate the boundaries between different cross-sectional regions. The carbon concentration and sp^3 depth profiles shown in Fig. 2 reveal the existence of the five regions: (i) *substrate* (the carbon signal intensity and sp^3 content are almost zero because this region corresponds to the NiTa layer); (ii) *interface layer* (both the carbon concentration and the sp^3 content show a sharp increase), (iii) *bulk film* (the carbon concentration stabilizes at ~100%, while the sp^3 fraction remains fairly constant); (iv) *surface layer* (both the carbon concentration and the sp^3 fraction show a sharp decrease); and (v) *capping layer* (the low carbon intensity is due to adventitious carbon physically adsorbed onto the surface of the Au capping layer). While 2-min Ar^+ ion irradiation barely affected the thickness and sp^3 content of the bulk layer, it significantly reduced the thickness of the interface and surface layers and shifted the carbon peak intensity deeper into the bulk layer.

Table 1 gives the thickness of the PECVD *a*-C film and each structural layer and the average sp^3 content of the bulk layer before and after Ar^+ ion irradiation for 2 min. The sum of the layer thicknesses is referred to as the film thickness. The agreement between TEM and EELS measurements of the film

thickness is fair. The average etching rate of PECVD *a*-C films predicted from EELS analysis is equal to ~0.9 nm/s, which is in excellent agreement with the HRTEM estimate. While sputter etching did not affect the bulk layer thickness, it reduced the thicknesses of the surface and interface layers from 2.0 to 0.9 nm and 2.0 to 1.4 nm, respectively, resulting in the decrease of film thickness from 5.5 to 3.7 nm. However, despite the significant decrease in film thickness, the effect of Ar^+ ion beam irradiation on the sp^3 content of the PECVD *a*-C films was secondary.

Fig. 3 shows cross-sectional HRTEM images of FCVA *a*-C films obtained before and after Ar^+ ion beam irradiation for 2 and 4 min. The dashed lines indicate the interfaces of the *a*-C film with the NiTa layer and evaporated Au capping layer. The images show a NiTa/*a*-C/Au/epoxy layered structure. The average film thickness measured from the TEM images shown in Fig. 3 is given in Table 1. The results show a decrease in film thickness due to Ar^+ ion beam irradiation for 2 and 4 min from 4.6 to 3.7 and 2.3 nm, respectively, representing an average etching rate of FCVA *a*-C films equal to ~0.5 nm/s.

Fig. 4 shows EELS results of FCVA *a*-C films obtained before and after Ar^+ ion beam irradiation for 2 and 4 min. Again, the normalized carbon intensity was obtained by integrating the EELS spectrum from 280 to 305 eV and then dividing by the peak intensity, while the sp^3 depth profiles were calculated from the corresponding C K-edge spectra using Eq. (1). Similar with the PECVD films, the EELS results shown in Fig. 4 reveal the existence of a multi-layer film structure consisting of interface layer, bulk film, and surface layer and a secondary effect of Ar^+ ion sputter etching on the sp^3 content of the bulk layer. However, the effect of sputter etching, especially for 4-min Ar^+ ion irradiation, on the film thickness and structure is significant. The trend is for the film thickness to decrease with increasing time of Ar^+ ion irradiation, mainly at the expense of the thickness of surface and interface layers.

As shown in Table 1, the agreement between TEM and EELS predictions of the as-deposited film thickness is fair. Ar^+ ion irradiation for 2 and 4 min resulted in the decrease of the average film thickness of FCVA *a*-C films from 5.8 to 4.9 and 3.6 nm, respectively, corresponding to an average etching rate of FCVA *a*-C films equal to ~0.5 nm/s, which is in excellent agreement with the HRTEM result. The lower

etching rate of FCVA films compared to PECVD films is attributed to the significantly higher (by ~22 at%) sp^3 content of the corresponding bulk layer (Table 1). While sputter etching during 2-min Ar^+ ion irradiation mainly caused thinning of the surface and interface layers, sputter etching during 4-min Ar^+ ion irradiation resulted in significant thinning of all the layers of FCVA *a*-C films. In particular, 2-min Ar^+ ion irradiation resulted in thinning of the surface, bulk, and interface layers by about 18%, 5.6%, and 22%, respectively, whereas for 4-min Ar^+ ion irradiation the corresponding thickness decrease was about 29%, 33%, and ~65%. Thus, it may be inferred that sputter etching during 2-min Ar^+ ion irradiation resulted in the decrease of the film thickness mainly due to the suppression of the surface and interface layers, whereas for sputter etching during 4-min Ar^+ ion irradiation all layers contributed significantly to the decrease of the film thickness. In addition, 4-min Ar^+ ion irradiation resulted in the decrease of the sp^3 content of the bulk layer by ~12 at%.

IV. CONCLUSIONS

The effect of Ar^+ ion beam irradiation on the structure, composition, and thickness of ultrathin *a*-C films deposited onto NiTa-coated glass substrates by PECVD and FCVA was examined by TEM and EELS. The results confirmed the existence of a multi-layer film structure consisting of interface, bulk, and surface layers of thickness in the range of 1–2.5 nm, depending on the deposition method and time of Ar^+ ion irradiation. While sputter etching during 2-min Ar^+ ion irradiation produced insignificant structural/compositional changes (e.g., sp^3 content), it induced significant thinning of the *a*-C films (about 28% and 16% for PECVD and FCVA films, respectively), mainly by reducing the thickness of the surface and interface layers and marginally the thickness of the bulk layer. However, sputter etching during 4-min Ar^+ ion irradiation resulted in significant thinning of all layers comprising the FCVA *a*-C films and a decrease of the sp^3 content by ~9%. The TEM and EELS results of this study demonstrate that *in-situ* Ar^+ ion beam irradiation is an effective post-deposition process for reducing the thickness of *a*-C films, without inducing significant structural changes.

ACKNOWLEDGMENTS

This research was funded by the Computer Mechanics Laboratory, University of California, Berkeley. The TEM/EELS studies were carried out at the National Center for Electron Microscopy, Molecular Foundry, Lawrence Berkeley National Laboratory (Proposal No. 1886). Work at the Molecular Foundry is supported by the Office of Science, Office of Basic Energy Sciences, U.S. Department of Energy (Contract No. DE-AC02-05CH11231).

REFERENCES

[1] A. Grill and B. Meyerson, "Development and status of diamondlike carbon," in *Synthetic Diamond: Emerging CVD Science and Technology*. New York, NY, USA: Wiley, 1994, pp. 91–141.

[2] J. Robertson, "Ultrathin carbon coatings for magnetic storage technology," *Thin Solid Films*, vol. 383, pp. 81–88, Feb. 2001.

[3] A. Anders, *Cathodic Arcs: From Fractal Spots to Energetic Condensation*. Springer Series on Atomic, Optical, and Plasma Physics, New York, NY, USA: Springer Science and Business Media, 2008.

[4] H.-S. Zhang and K. Komvopoulos, "Surface modification of magnetic recording media by filtered cathodic vacuum arc," *J. Appl. Phys*., vol. 106, no. 9, pp. 093504-1–093504-7, Nov. 2009.

[5] S. Xu, B. K. Tay, H. S. Tan, L. Zhong, Y. Q. Tu, S. R. P. Silva, and W. I. Milne, "Properties of carbon ion deposited tetrahedral amorphous carbon films as a function of ion energy," *J. Appl. Phys*., vol. 79, no. 9, pp. 7234–7240, May 1996.

[6] E. Riedo, F. Comin, J. Chevrier, F. Schmithusen, S. Decossas, and M. Sancrotti, "Structural properties and surface morphology of laser-deposited amorphous carbon and carbon nitride films," *Surf. Coat. Technol.*, vol. 125, no. 1, pp. 124–128, March 2000.

[7] D. Wan and K. Komvopoulos, "Transmission electron microscopy and electron energy loss spectroscopy analysis of ultrathin amorphous carbon films," *J. Mater. Res.*, vol. 19, no. 7, pp. 2131–2136, July 2004.

[8] N. Wang and K. Komvopoulos, "The multilayered structure of ultrathin amorphous carbon films synthesized by filtered cathodic vacuum arc deposition," *J. Mater. Res*., vol. 28, no. 16, pp. 2124–2131, Aug. 2013.

[9] L. K. Cheah, X. Shi, E. Liu, and B. K. Tay, "Electron field emission properties of tetrahedral amorphous carbon films," *J. Appl. Phys.*, vol. 85, no. 9, pp. 6816–6821, May 1999.

[10] P. Patsalas and S. Logothetidis, "Surface and bulk microstructural modifications in amorphous carbon films after post-growth low energy ion beam irradiation," *MRS Proc.,* vol. 650, pp. R3.42.1–R3.42.6, Nov. 2001.

[11] P. Patsalas and S. Logothetidis, "The effect of postgrowth ion irradiation on the microstructure and the interface properties of amorphous carbon films on silicon," *J. Appl. Phys.*, vol. 88, no. 11, pp. 6346–6354, Dec. 2000.

[12] M. Silinskas and A. Grigonis, "Low energy post-growth irradiation of amorphous hydrogenated carbon (a-C:H) films," *Diamond Rel. Mater.*, vol. 11, no. 3, pp. 1026–1030, March 2002.

[13] M. Vinnichenko, R. Gago, N. Huang, Y. X. Leng, H. Sun, U. Kreissig, M. P. Kulish, and M. F. Maitz, "Spectroscopic ellipsometry investigation of amorphous carbon films with different sp^3 content: relation with protein adsorption," *Thin Solid Films*, vols. 455–456, pp. 530–534, May 2004.

[14] H.-S. Zhang and K. Komvopoulos, "Direct-current cathodic vacuum arc system with magnetic-field mechanism for plasma stabilization," *Rev. Sci. Instrum.*, vol. 79, no. 7, pp. 073905-1–073905-7, July 2008.

[15] H.-S. Zhang and K. Komvopoulos, "Synthesis of ultrathin carbon films by direct current filtered cathodic vacuum arc," *J. Appl. Phys*., vol. 105, no. 8, pp. 083305-1–083305-7, April 2009.

[16] J. Xie and K. Komvopoulos, “Structural stability of ultrathin amorphous carbon films subjected to rapid thermal annealing,” submitted.

[17] J. Xie and K. Komvopoulos, “The role of duty cycle of substrate pulse biasing in filtered cathodic vacuum arc deposition of amorphous carbon films,” *IEEE Trans. Magn.*, vol. 51, no. 12, pp. 3302009-1–3302009-9, Dec. 2015.

[18] D. Wan and K. Komvopoulos, “Transmission electron microscopy and electron energy loss spectroscopy analysis of ultrathin amorphous carbon films,” *J. Mater. Res*., vol. 19, no. 7, pp. 2131–2136, July 2004.

[19] N. Wang and K. Komvopoulos, “Incidence angle effect of energetic carbon ions on deposition rate, topography, and structure of ultrathin amorphous carbon films deposited by filtered cathodic vacuum arc,” *IEEE Trans. Magn*., vol. 48, no. 7, pp. 2220–2227, July 2012.

[20] D. B. Williams and C. B. Carter, *Transmission Electron Microscopy: A Textbook for Materials Science*. New York, NY, USA: Springer-Verlag, 2009, ch. 37, pp. 679–681.

[21] R. F. Egerton, *Electron Energy-Loss Spectroscopy in the Electron Microscope*. 3rd ed., New York, NY, USA: Springer-Verlag, 2011, ch. 3, pp. 111–229.

[22] J. J. Cuomo, J. P. Doyle, J. Bruley, and J. C. Liu, “Sputter deposition of dense diamond-like carbon films at low temperature,” *Appl. Phys. Lett*., vol. 58, no. 5, pp. 466–468, Feb. 1991.

Table 1. Film thickness, surface, bulk, and interface layer thickness, and average sp^3 content of bulk layer of *a*-C:H and *a*-C films deposited by PECVD and FCVA, respectively, obtained before (as-deposited) and after Ar^+ ion beam irradiation for 2 and 4 min.

Measurement	Film (deposition method)					
	a-C:H (PECVD)			*a*-C (FCVA)		
	as-deposited	Ar^+ ion irradiated[(a)]		as-deposited	Ar^+ ion irradiated[(a)]	
		2 min	4 min		2 min	4 min
Film thickness[(b)] (nm)	4.6 ± 0.2	2.8 ± 0.4	1.1 ± 0.3	4.6 ± 0.1	3.7 ± 0.3	2.3 ± 0.3
Film thickness[(c)] (nm)	5.5	3.7	–	5.8	4.9	3.6
Surface layer thickness[(c)] (nm)	2.0	0.9	–	1.7	1.4	1.2
Bulk layer thickness[(c)] (nm)	1.5	1.4	–	1.8	1.7	1.2
Interface layer thickness[(c)] (nm)	2.0	1.4	–	2.3	1.8	1.2
Average sp^3 in bulk layer[(c)] (at%)	37.6 ± 0.4	36.6 ± 0.4	–	59.1 ± 1.4	57.5 ± 1.9	51.9 ± 1.4

[(a)]Ion kinetic energy = 500 eV, ion incidence angle = 30°, working pressure = 2×10^{-4} Torr; [(b)]TEM; [(c)]EELS

List of Figures

Fig. 1 Cross-sectional HRTEM images of *a*-C:H films deposited by PECVD obtained (a) before and after Ar^+ ion beam irradiation for (b) 2 min and (c) 4 min. Contrast and structure differences reveal the following regions: (1) NiTa layer, (2) *a*-C film, (3) Au capping layer, and (4) epoxy mounting material (marked only in (b)).

Fig. 2 Depth profiles of normalized carbon intensity and sp^3 content calculated from the C K-edge spectra of *a*-C:H films deposited by PECVD. The figure shows variations in the film structure (a) before and (b) after Ar^+ ion beam irradiation for 2 min. The boundaries between different regions are distinguished by dashed lines.

Fig. 3 Cross-sectional HRTEM images of *a*-C films deposited by FCVA obtained (a) before and after Ar^+ ion beam irradiation for (b) 2 min and (c) 4 min. Contrast and structure differences reveal the following regions: (1) NiTa layer, (2) *a*-C film, (3) Au capping layer, and (4) epoxy mounting material (marked only in (b)).

Fig. 4 Depth profiles of normalized carbon intensity and sp^3 content calculated from the C K-edge spectra for *a*-C films deposited by FCVA. The figure shows variations in the film structure (a) before and after Ar^+ ion beam irradiation for (b) 2 min and (c) 4 min. The boundaries between different regions are distinguished by dashed lines.

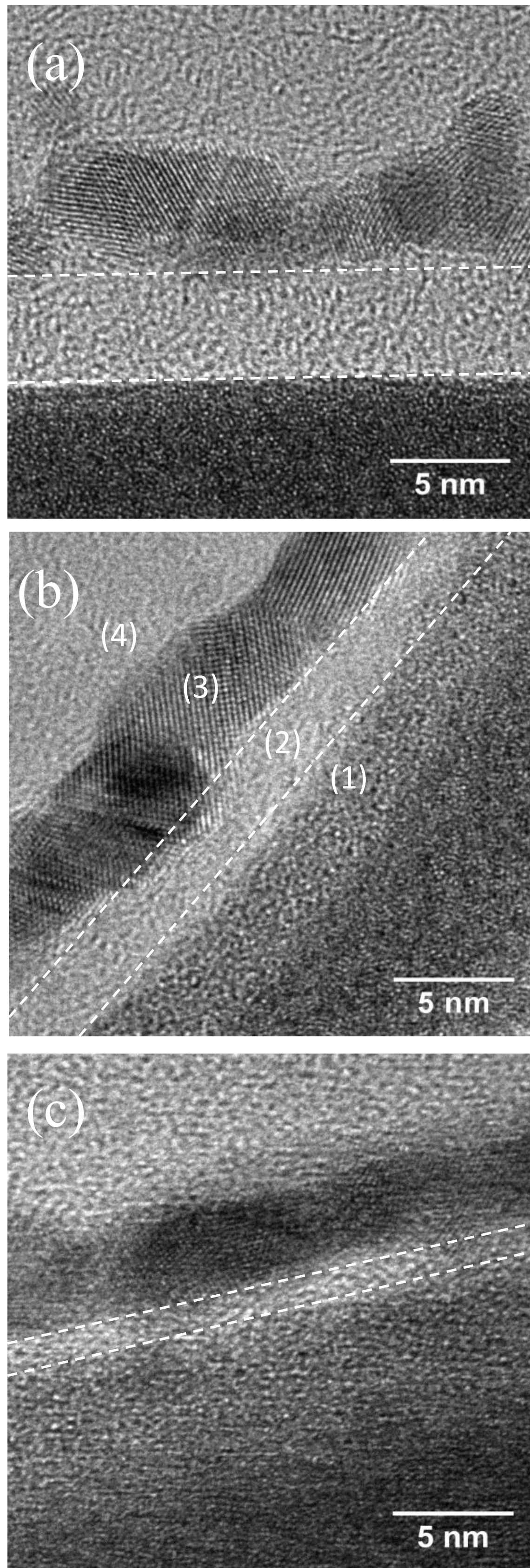

Figure 1

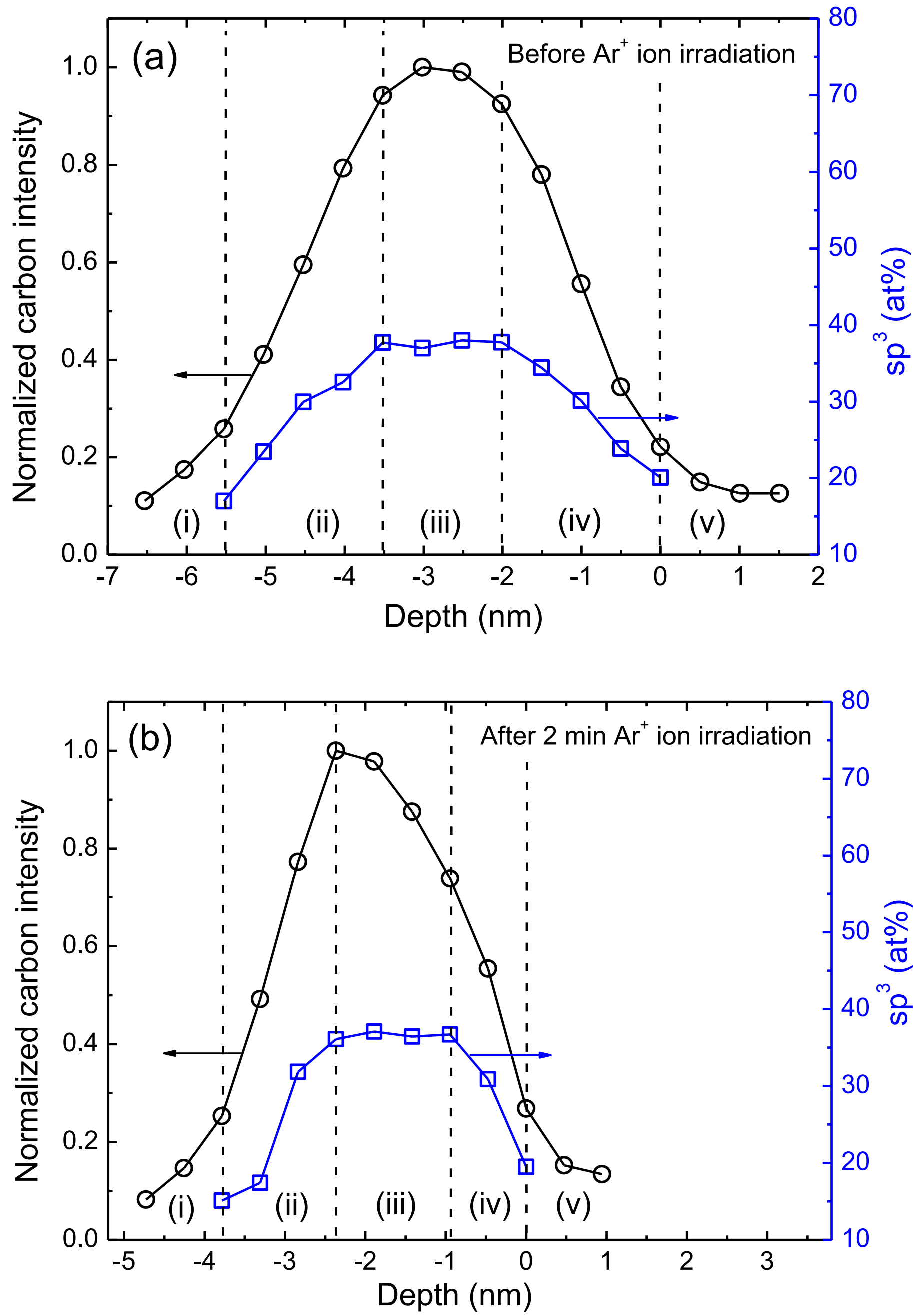

Figure 2

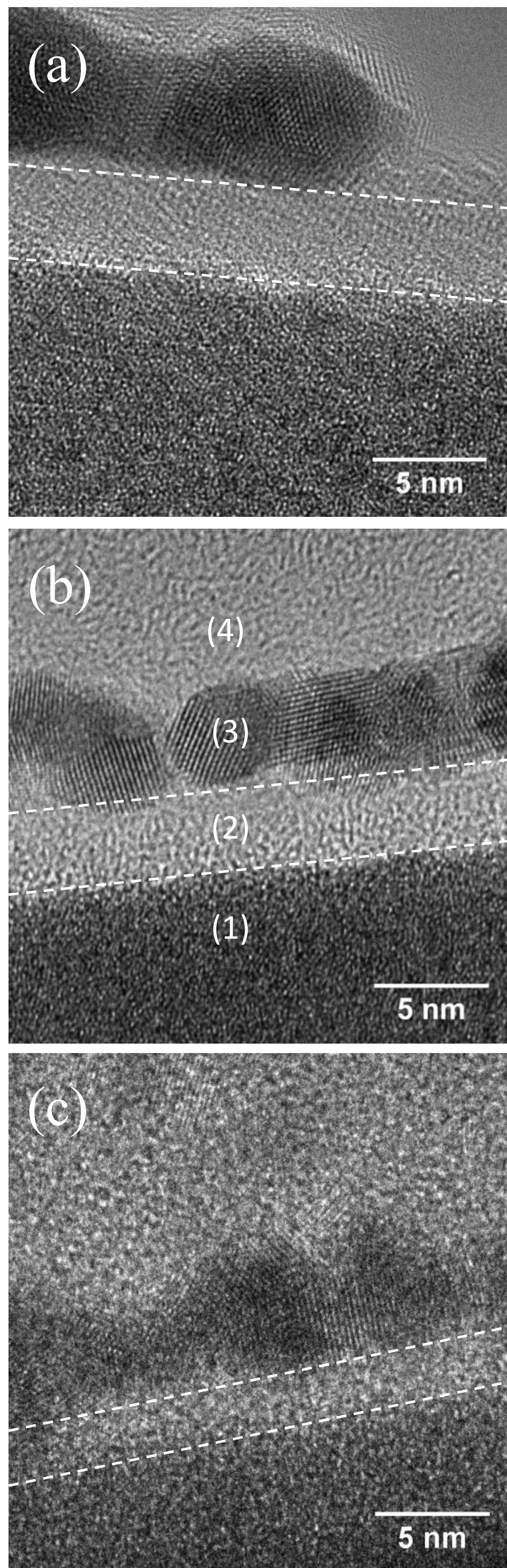

Figure 3

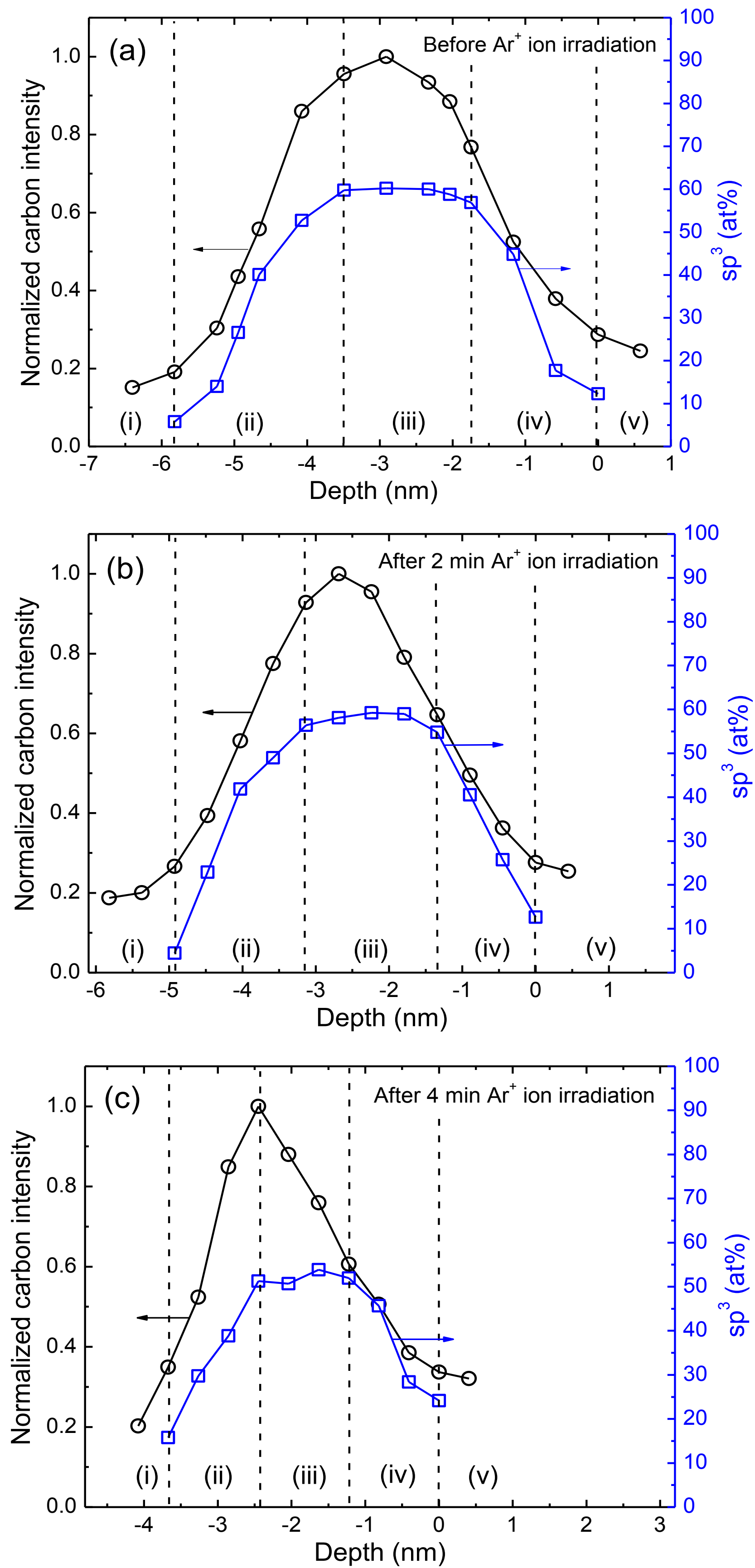

Figure 4